distances in the pyridine rings. No shortening of the bond lengths C(1)–C(2) and C(4)–C(5) in the pyridine rings was observed.

We are greatly indebted to Prof L. G. Sillén, Director of the Department of Inorganic Chemistry of the Royal Institute of Technology in Stockholm, for his help and interest in this work. We are most thankful to Dr G. Lundgren for his friendly help and also to Dr D. MacWhan. Dr J. Šmogrovič was kind enough to supply us with the crystals of monopyridine-copper(II) acetate.

Last but not least, we wish to thank the Swedish Board of Computing Machinery for providing us with free time on the computers BESK and FACIT EDB.

References

ÅSBRINK, S., BLOMQVIST, G. & WESTMAN, S. (1961). *Ark. Kemi*, **14**, 545.
ÅSBRINK, S. & BRÄNDÉN, I. (1963). To be published.
BARCLAY, G. A. & KENNARD, C. H. L. (1961). *J. Chem. Soc.* p. 5244.
BERGHUIS, J., HAANAPPEL, IJ. M., POTTERS, M., LOOPSTRA, B. O., MACGILLAVRY, C. H. & VEENENDAAL, A. L. (1955). *Acta Cryst.* **8**, 478.
HANIC, F., ŠTEMPELOVÁ, D. & HANICOVÁ, K. (1961) *Chemické Zvesti.* **15**, 102.
HUGHES, E. W. (1941). *J. Amer. Chem. Soc.* **63**, 1737.
MARTIN, R. L. & WATERMAN, H. (1959). *J. Chem. Soc.* p. 2960.
NIEKERK, J. N. VAN & SCHOENING, F. R. L. (1953). *Acta Cryst.* **6**, 227.

Acta Cryst. (1964). **17**, 639

Precise and Accurate Lattice Parameters by Film Powder Methods. III. An Exact Graphical Method for Axial (Vertical) Divergence Profiles for Cylindrical Diffraction Cameras*

BY K. E. BEU, D. K. LANDSTROM
Development Laboratory, Physical Measurements Department, Goodyear Atomic Corporation, Piketon, Ohio, U.S.A.

D. R. WHITNEY
Ohio State University, Columbus, Ohio, U.S.A.

AND E. R. PIKE
Royal Radar Establishment, Malvern, Worcestershire, England

(*Received* 14 *February* 1962 *and in revised form* 1 *August* 1963)

An exact graphical method has been developed for calculating axial divergence profiles for cylindrical powder cameras. The method is exact in that no approximations are used in deriving the equations for calculating the profiles. The profiles can easily be plotted with an accuracy considerably greater than the best precision with which diffraction lines can be measured on film patterns (about 0·002° θ (Straumanis & Ievins, 1940)). This is important when these profiles are used to correct diffraction line measurements for axial divergence, so that the application of this systematic error correction will not limit the accuracy of the corrected data.

Various characteristics of axial divergence profiles for cases of practical interest are presented. In particular, it is shown that the use of extremely high angles (about 175° 2θ) as recommended by Straumanis & Weng (1955) causes negligible error (less than the 0·002° θ precision of measurement possible with sharp diffraction lines) due to axial divergence, provided the collimator dimensions are restricted as described, a spot focus source is used, and diffraction measurements are made in the equatorial plane of the diffraction pattern. Relaxation of these conditions may require correction for axial divergence; however, for cameras of the type described by Straumanis (not necessarily identical with Straumanis-type cameras), the correction for axial divergence will usually be less than the precision of measurement and may be neglected.

1. Introduction

The problem of axial (vertical) divergence has been treated in numerous ways with varying degrees of approximation and various quantitative conclusions. It is, however, generally agreed that: (1) the correction for axial divergence increases as 2θ approaches either 0° or 180°, and (2) the correction goes to zero in the range of about 90° to 120° 2θ (Eastabrook, 1952; Pike, 1957). Methods for calculating axial divergence profiles have been derived for two crystal X-ray

* This work (other than the contribution by Dr E. R. Pike) was performed under Contract AT-(33-2)-1 with the U.S. Atomic Energy Commission.

spectrometers (Schwarzschild, 1928; DuMond & Hoyt, 1930; Spencer, 1931); however, these are not directly applicable to diffractometer or film powder techniques. Lipson & Wilson (1941) have derived an espression for powder cameras for the change in 'd' due to axial divergence which reduces to a particular form of Eastabrook's (Eastabrook, 1952) equation 12. Alexander (1950, 1954) has developed expressions for axial divergence profiles for diffractometers based on certain simplifying assumptions. Eastabrook (1952) has presented an axial divergence profile for diffractometers, and Pike (1957) has developed expressions for the centroid shift of axial divergence diffractometer profiles. Thus, no quantitative methods have been presented which permit calculation of axial divergence profiles directly for film powder cameras.

It is a purpose of this article to present a graphical method for calculating axial divergence profiles based on experimentally realizable conditions using precisely built cylindrical-film powder cameras. The method is exact in that no approximations are used in the derivation, the accuracy of the final profile depending primarily on the intervals used in the graphical solution. The profiles thus obtained are convoluted with other error profiles and with Cauchy profiles, representing spectral and particle size broadening distributions, to determine the shift of the diffraction maxima due to the error profiles. These shifts are then applied as corrections to the measured diffraction line positions to permit calculations of $\hat{\hat{a}}_0$, the maximum likelihood estimate of the lattice parameter under the hypothesis of 'no remaining systematic errors' within the precision of the Bragg angle measurements, using the likelihood ratio method or LRM (Beu, Musil & Whitney, 1962). This approach is called the convolution-film method (Beu, 1963).

The profiles to be presented are based on a practical case involving the dimensions of a precisely built 57·6 mm powder camera to aid in evaluating the need for axial divergence corrections. In some cases the profiles are plotted on a scale which can be read to 0·0001° 2θ. It should not be inferred from this that diffraction line measurements can be read with this precision when this or other film cameras are used. Rather, it should be recalled (Straumanis & Ievins, 1940) that lines can be read on film with a precision no better than about 0·002° θ. Nevertheless, it is desirable to obtain error profiles with an accuracy better than measurement precision so that measurement precision, rather than the systematic correction based on the error profile, will limit the accuracy attainable in the final lattice parameter calculation.

2. Assumptions

In the development of this method for calculating axial divergence profiles, the assumptions are made that (1) the X-ray source is a line of uniform brightness of length $2a$, and (2) the sample is a line of length $2b$ parallel to the source (Fig. 1). The radial factors (source intensity distribution perpendicular to the line focus and radial (horizontal) divergence and absorption of the X-ray beam for a finite sample diameter) are handled separately by the Taylor–Sinclair line contour matrix method (Taylor & Sinclair, 1945) and convoluting the resultant profiles with the axial divergence profile. This provides an accurate estimate of the combined effects of these error profiles since the axial divergence profile is calculated in the same plane (*e.g.* the equatorial) as the radial divergence, absorption, and source profiles.

Uniformity of brightness along the line focus (at least 3 to 5 mm) has been observed within 1 or 2% in several sealed-off copper target X-ray diffraction tubes as determined by examining microphotometer scans of pinhole images of the line focus. Uniformity of the cylindrical powder sample along its length can be readily achieved with careful sample preparation, especially when glass capillaries are used, provided the sample particle size is small enough to be in the range for sharp diffraction lines. Parallelism of source and sample is achieved to the required degree by normal camera alignment procedures. Thus, these assumptions are consistent with experimentally attainable conditions. Having carried out the derivation based on these assumptions, the method can be extended to include spot focus source conditions, as will be discussed in § 4(*c*).

3. Calculation procedure

With the geometrical line source and line sample just described, calculations of the intensity profile due to axial divergence alone will be developed based on the nomenclature of Fig. 1. The X-ray line source is parallel to the x axis such that a sample of length $2b$ on the x axis sees only that portion of the source between $+a$ and $-a$ as defined by the collimator system. The intensity I_α at the point R_α on the equatorial plane of the film cylinder of radius OR is the sum of the intensities of all rays leaving points $(f, s, 0)$ on the source, irradiating the sample at points $(p, 0\ 0)$ and diffracting through an angle $2\psi (2\psi = 180° - 2\theta)$ to point R_α on the film cylinder subject to the collimator restrictions. The collimator dimensions of interest are defined by the points $(\pm x_1, y_1, 0)$ and $(\pm x_2, y_2, 0)$. Values of I_α are calculated for a range of values of the angle α, where α is the angle ROR_α in the equatorial plane. A plot of I_α versus α then gives the axial divergence profile along the equatorial plane of the film cylinder* where the true 2ψ angle unaffected by axial divergence corresponds to the ray from Y to O to R_α; *i.e.* $2\psi = \alpha$. Calculations of I_α versus α are made as follows:

* Off-axis profiles where $r \neq 0$ (non-equatorial planes of the film cylinder) may also be obtained, as will be discussed in § 4(*d*).

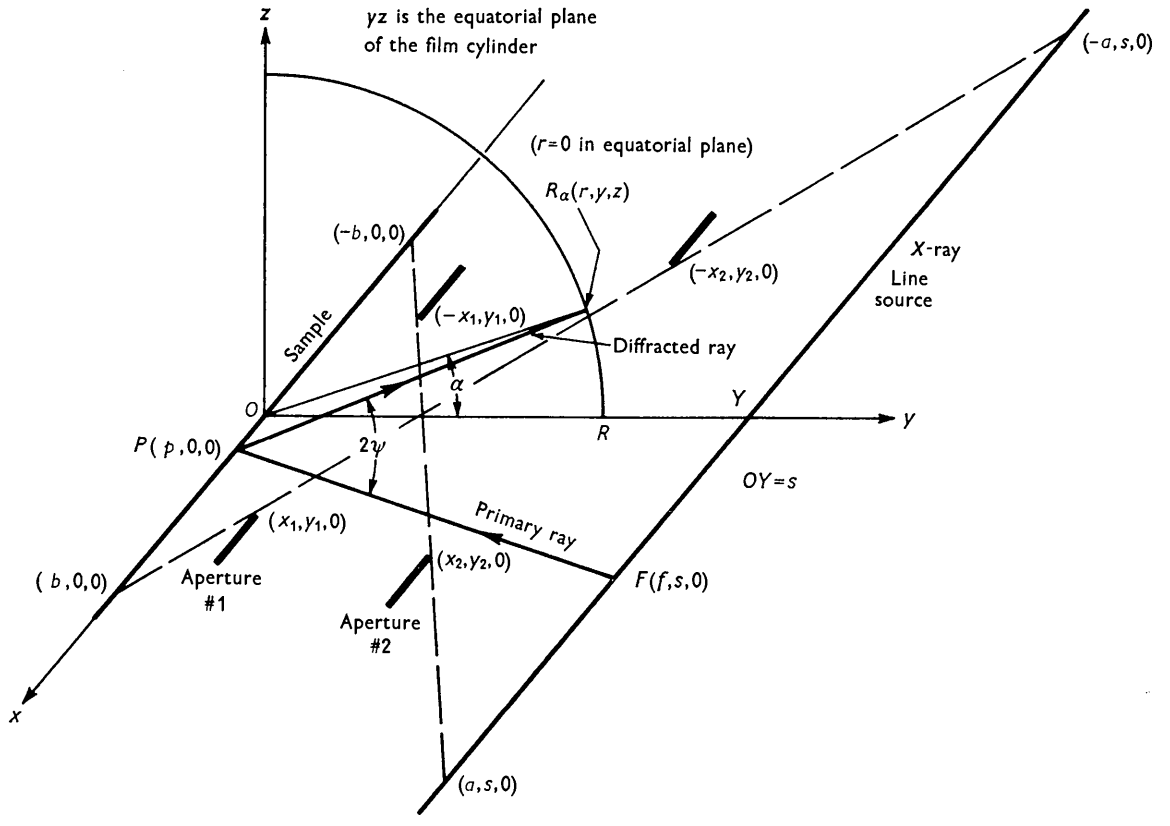

Fig. 1. Schematic of cylindrical camera illustrating axial divergence.

The film cylinder centered on $x=0$ is defined by:

$$y^2+z^2=R^2\,.$$

The angle 2ψ between a primary ray FP and its diffracted ray PR_α is given in terms of direction cosines:

$$\cos 2\psi=\frac{(f-p)(r-p)+ys}{\sqrt{((f-p)^2+s^2)}\sqrt{((r-p)^2+y^2+z^2)}}\,. \quad (1)\dagger$$

This equation can be rewritten in the form $ax^2+bx+c=0$ as follows:

$$[R^2\cos^2 2\psi-(r-p)^2\sin^2 2\psi](f-p)^2-2[ys(r-p)](f-p)+s^2[(r-p)^2\cos^2 2\psi+R^2\cos^2 2\psi-y^2]=0\,. \quad (2)$$

Solving equation (2) for $(f-p)$ and substituting $y=R\cos\alpha$, we obtain:

$$f=p+\frac{(sR\cos\alpha)(r-p)\pm s\cos 2\psi\sqrt{([R^2+(r-p)^2][R^2\cos^2\alpha-R^2\cos^2 2\psi+(r-p)^2\sin^2 2\psi])}}{R^2\cos^2 2\psi-(r-p)^2\sin^2 2\psi}\,. \quad (3)$$

Designating: $(sR\cos\alpha)(r-p)=M$

$$s\cos 2\psi\sqrt{([R^2+(r-p)^2][R^2\cos^2\alpha-R^2\cos^2 2\psi+(r-p)^2\sin^2 2\psi])}=N$$

$$R^2\cos^2 2\psi-(r-p)^2\sin^2 2\psi=Q\,.$$

† This equation is equivalent to Eastabrook's equation (6) (Eastabrook, 1952).

Equation (3) may be simplified as follows:

$$f_{1\alpha}=p+g_\alpha(p)+h_\alpha(p) \quad (4)$$

$$f_{2\alpha}=p+g_\alpha(p)-h_\alpha(p) \quad (5)$$

where:

$$g_\alpha(p)=M/Q$$
$$h_\alpha(p)=N/Q\,.$$

These equations are subject to the collimator restrictions, assuming the X-ray beam fills the collimator system:

$$y_1f+(s-y_1)p+x_1s\geq 0 \quad (6)$$

$$y_2f+(s-y_2)p+x_2s\geq 0 \quad (7)$$

$$y_1f+(s-y_1)p-x_1s\leq 0 \quad (8)$$

$$y_2f+(s-y_2)p-x_2s\leq 0\,. \quad (9)$$

Inequalities (6) to (9) define region C (Fig. 2) in the plane* such that any point (f, p) in C corresponds to a pair of rays from F to P to R_α where angle $FPR_\alpha=2\psi$ (Fig. 1). The intensity at R_α is:

$$I_\alpha=|f_{1\alpha}|C+|f_{2\alpha}|C \quad (10)$$

* Note that negative f values are plotted to the right of the origin in Fig. 2.

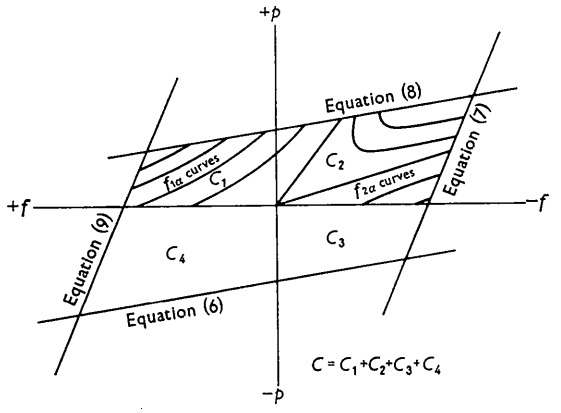

Fig. 2. Region C in $[f, p]$ plane bounded by lines due to collimator restrictions and showing a few $f_{1\alpha}$ and $f_{2\alpha}$ curves ($2\theta = 160°$, $r = 0$). Equation numbers correspond to those in the text on page 641.

where $|f_{1\alpha}|C$ and $|f_{2\alpha}|C$ represent the areas of strips for a given (average) value of α in the $[f, p]$ plane. The f_α strips are of constant angular width $\Delta\alpha$ and are bounded by region C. The total area of corresponding $f_{1\alpha}$ and $f_{2\alpha}$ strips for a given value of α represents the intensity of the profile at that value of α. The accuracy of the profile intensity values depends (*a*) on the accuracy with the f_α curves are drawn, (*b*) on the accuracy with which the f_α strip areas are measured, and (*c*) on the interval used for $\Delta\alpha$. We have found that intensities can be measured reproducibly to about 1% by plotting the f_α curves on $11'' \times 17''$ graph paper and measuring the areas with a planimeter. In the example cited, an interval, $\Delta\alpha = 0{\cdot}0005°\ 2\theta$, can be readily measured and permits points to be obtained as close as $0{\cdot}00025°\ 2\theta$ to the $\Delta 2\theta = 0°(2\varepsilon = 0)$ position. The accuracy of this graphical method will be brought out in the following paper (Part IV) in which profile data which were obtained both graphically and analytically will be compared.

Since subregions C_3 and C_4 (Fig. 2) are related to subregions C_1 and C_2 by a center of symmetry at the origin, for equatorial profiles, I_α is also given by:

$$I_\alpha = 2|f_{1\alpha}|C_1 + 2|f_{2\alpha}|C_2 \,. \qquad (11)$$

The use of equation (11) instead of (10) cuts the computation requirements in half. Since only relative intensity values are of interest, the factor of two in equation (11) may be dropped. Computations may be further simplified by rotating subregion C_2 through 180° about the origin so that the $f_{1\alpha}$ strips of C_1 join the corresponding $f_{2\alpha}$ strips of C_2 (Fig. 3). equation 11 can then be evaluated directly for the I_α's by measuring the areas of the now continuous $f_{1\alpha}+f_{2\alpha}$ strips. Plotting I_α *versus* α then gives the axial divergence profile.

In practice, equations (4) and (5) are solved for (f, p) values as a function of α with the use of an IBM 1410 computer. The $f_{1\alpha}$ and $f_{2\alpha}$ curves are plotted from these data as shown in Fig. 3 after the collimator boundaries have been calculated. For the sake of clarity, only a few f_α curves are shown.

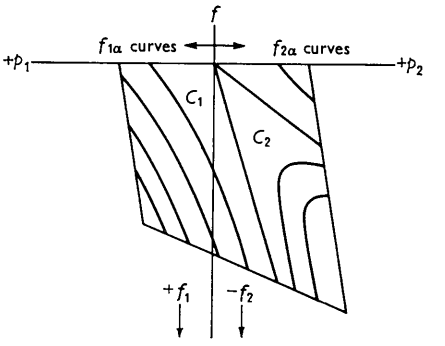

Fig. 3. Rearrangement of subregions C_1 and C_2 for more convenient measurement of f_α strip areas.

4. Axial divergence profiles for a precision 57·6 mm camera

(*a*) *Camera geometry*

A Philips 57·6 mm, diameter camera was rebuilt into a precision Straumanis-type camera and is described elsewhere (Beu, Musil & Scott, 1962). Axial divergence profiles for this camera will be presented since the pertinent dimensions are representative of many precision cameras of this type. These dimensions are as follows (Fig. 1):

First aperture (pinhole)	$x_1 = 0{\cdot}25$ mm, $-x_1 = 0{\cdot}25$ mm, $y_1 = 6{\cdot}8$ mm.
Second aperture (slit)	$x_2 = 0{\cdot}50$ mm, $-x_2 = 0{\cdot}50$ mm, $y_2 = 49{\cdot}8$ mm.
Camera radius	$R(=OR) = 28.8$ mm.
Sample-target distance	$s(=OY) = 95{\cdot}5$ mm.

(*b*) *Line focus profiles*

Fig. 4 shows axial divergence profiles in the equatorial plane for this camera in the range of 2θ from 5° to 175° using a line focus source (Fig. 4(*a*) for the 45° to 160° and Fig. 4(*b*) for the 5° to 175° range because of the large difference in scale required for the abscissa. Note that $\Delta 2\theta(=-2\varepsilon) = 0{\cdot}0000°$ corresponds to the reference 2θ value given in the central regions of these graphs). Pike & Wilson (1959) pointed out that instrumental aberration functions are approximately triangular and this can be observed for the axial divergence profiles of Fig. 4. In addition, the exact profiles of Fig. 4 have the following features:

1. The maxima of all equatorial profiles occur at $\Delta 2\theta = 0$.

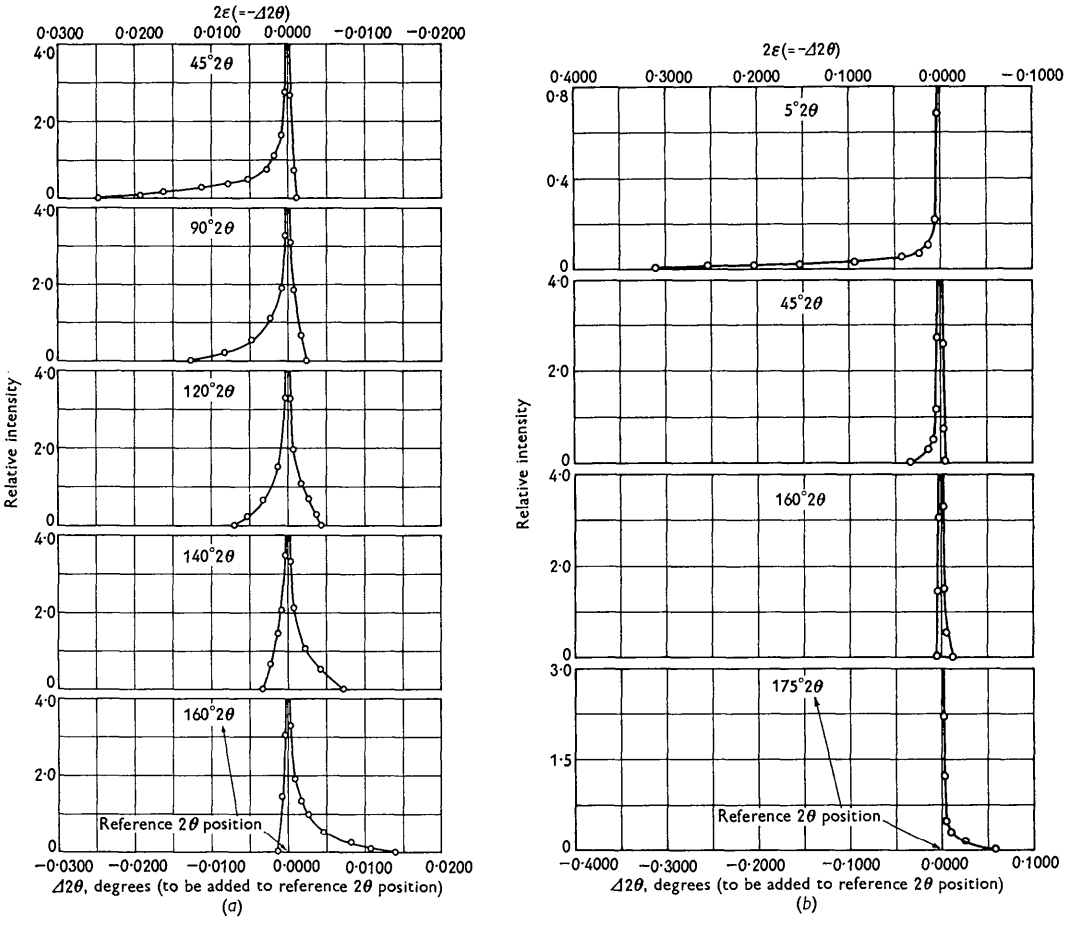

Fig. 4. Axial divergence profiles in the equatorial plane ($r=0$) for precision 57·6 mm powder camera using line focus (*a*) 45° to 160° 2θ, (*b*) 5° to 175° 2θ.

2. There is measurable intensity on either side* of $\Delta 2\theta=0$. (There is intensity to $0{\cdot}0001°\Delta 2\theta$ for the 5° 2θ profile and to $-0{\cdot}0003°\Delta 2\theta$ for the 175° 2θ profile. These intensities cannot be seen on the graphs because of the scale used.)
3. The profile curves rise to infinity† from either side of $\Delta 2\theta=0$. The infinity would be observed in the ideal case if an infinitely narrow detector slit or infinitely small photographic grains in the X-ray film were available for detecting the intensity at $\Delta 2\theta=0$. Any departure from these conditions would result in a finite amount of power being received at the detector. In addition, the lack of microscopic uniformity of the source and sample in the physical case would entirely eliminate the possibility of an infinity.‡

* Intensity is shown to occur on only one side of $\Delta 2\theta=0$ in the axial divergence profile of Eastabrook (1952) and is implied to be so by Alexander (1948). This is because Eastabrook used the assumption of a point source and point receiver in deriving his intensity equation (15) and Alexander used the implicit assumption of a parallel beam of X-rays. Neither of these restrictions apply to the derivation given in this paper.

† This will be shown analytically in the following paper (Part IV).

(*c*) *Spot focus profiles*

When a 1 mm × 10 mm X-ray source is viewed in the spot focus direction, the 1 mm width of the source and the first aperture (Fig. 1) completely define the maximum axial divergence of the X-ray beam reaching the sample. In this case the profile is considerably narrower than when both apertures are completely filled with radiation as they are when the source is viewed in the line focus direction. This may be seen by comparing 160° 2θ line and 'spot' focus profiles (not illustrated). A 'spot' focus profile is actually a line focus profile calculated for a line source having a width equivalent to the narrow dimension of the focal spot. Two 'spot' focus profiles were calculated with a line source length of 1 mm and OY distances (Fig. 1) of 90·5 and 100.5 mm. These latter two dimensions

‡ L. E. Alexander (private communication, 1962).

correspond to the distances of the extremities of the long axis of the 1 mm × 10 mm focal spot to the sample axis when viewed in the spot focus direction.

The two spot focus profiles are nearly identical and resemble the 160° 2θ line focus profile of Fig. 4(*a*), except that their total widths are only 0.004° 2θ. Their centroids* are displaced the same distance with negligible error (less than 0.0001° 2θ) from the reference 160° 2θ position. (The displacement of the spot focus centroid ($\Delta 2\theta = 0{\cdot}0004°$ 2θ) is much less than it is for the line focus profile ($\Delta 2\theta = 0{\cdot}0022°$ 2θ).)

From these observations it can be seen that spot focus profile shapes and centroid positions are relatively insensitive to small variations in OY distance. Thus, axial divergence profiles may be accurately calculated for either spot or line focus sources and this accuracy is well within the best precision claimed in the literature for lattice parameter measurements (about 0·001° 2θ).

(*d*) *Non-equatorial profiles*

The profiles discussed in the previous sections were calculated for intensities in the equatorial plane only ($r=0$, Fig. 1). These axial divergence profiles are of interest when diffraction line positions are measured visually since visual measurements are usually made along the line defined by the intersection of the equatorial plane with the film cylinder. On the other hand, if line positions are measured from microphotometer charts of the diffraction film, non-equatorial ($r \neq 0$) profiles are of interest since the microphotometer slit scans over a finite range on either side of the equatorial plane. The non-equatorial profiles can be calculated as readily as those for $r=0$; however, the entire C region in the $[f,p]$ plane (Fig. 2) is required to measure the f_α strip areas, since the center of symmetry is no longer at the origin.

Fig. 5 illustrates 160° 2θ line focus profiles for the collimator dimensions given in § 4(*a*) for $r=0$, 0·5 and 1·0 mm. The non-equatorial profiles broaden out rapidly and move away completely from the 160° 2θ position. From this it can be seen that, unless an X-ray diffraction line position is measured exactly along the equator, the effect of axial divergence may be much more pronounced than is indicated by the equatorial profiles shown in Fig. 4. The axial divergence profile which a microphotometer slit 2·0 mm long sees would be a composite of all profiles between $r=0$ and $r = \pm 1{\cdot}0$ mm. No attempts have been made to prepare such composite profiles; however, the process would be completely straightforward, though somewhat tedious.

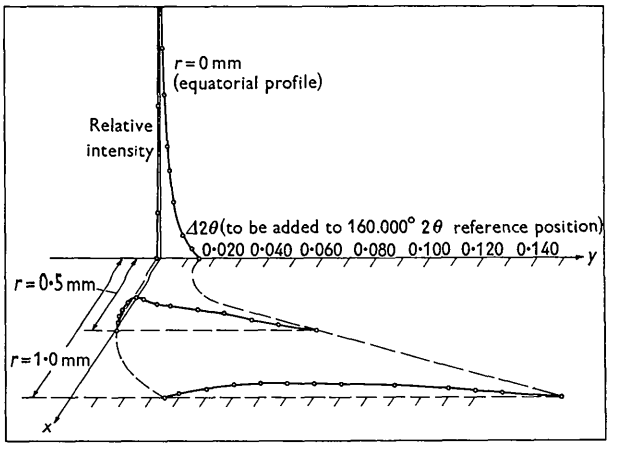

Fig. 5. Non-equatorial axial divergence profiles for 160° 2θ.

* Centroids were calculated by the use of equation (36) of Part IV.

5. Analysis of Straumanis's data at high angles

Axial divergence is a systematic error factor not discussed explicitly by Straumanis & Ievins (1940) and, since they claim to have eliminated systematic errors experimentally, it seems worth while to investigate the contribution of axial divergence to some of Straumanis's lattice parameter data, especially those at very high diffraction angles. In reporting the lattice constant of chromium Straumanis & Weng (1955) used the 321 diffraction line at about 175° 2θ for Cu $K\alpha_1$ radiation.

The axial divergence profile at 175° 2θ and in the equatorial plane was calculated using the collimator and camera dimensions reported (Straumanis & Ievins, 1940; Straumanis & Weng, 1955). Convoluting this profile with a Cauchy profile of 1·40° 2θ half-width (representing the convolution of appropriate spectral and crystallite size distribution profiles), the peak of the convoluted profile* is shifted by 0·002° from the reference 2θ position. This is less than the precision of measurement of about 0·002° θ claimed (Straumanis & Ievins, 1940). Hence, Straumanis & Weng were justified in neglecting axial divergence even at the very high angle of 175° 2θ.

The general statement can be made that corrections for axial divergence may be neglected in the 2θ range of interest (120° to 175°) for most lattice parameter measurements of high precision and accuracy when a spot focus source is used with collimator geometry similar to that described (Straumanis & Weng, 1955), and when measurements are made in the equatorial plane. If these conditions are not met, then it is advisable to calculate the appropriate axial divergence profile to determine if such a profile, when convoluted with other pertinent profiles, causes a significant shift from the reference diffraction profile position.

* This convoluted profile represents the experimentally observed profile if axial divergence were the only factor distorting the pure diffraction plus spectral profile. Other factors such as Lorentz and polarization, absorption, *etc.*, may also affect the profile shape but they are not included since the only factor of interest here is axial divergence.

Thanks are due to J. I. Langford for many helpful discussions and to Dr. L. E. Alexander and Prof. A. J. C. Wilson for their interest in this project. Thanks are also due to R. E. Entler, F. J. Musil, K. Ralston, N. L. Scott, F. C. Steinbach, J. P. Wilkins and G. J. Williams for the many calculations involved.

References

ALEXANDER, L. (1948). *J. Appl. Phys.* **19**, 1068.
ALEXANDER, L. (1950). *J. Appl. Phys.* **21**, 126.
ALEXANDER, L. (1954). *J. Appl. Phys.* **25**, 155.
BEU, K. E. (1963). *X-ray diffraction methods with estimates of accuracy and precision of these methods.* G. L. Clark, ed. *The encyclopedia of X-rays and gamma rays.* p. 709. New York: Reinhold.
BEU, K. E., MUSIL, F. J. & SCOTT, D. L. (1962). *Modifications of a commercial cylindrical powder diffraction camera for precise and accurate lattice parameter measurements.* USAEC Report GAT-T-973, Goodyear Atomic Corp.
BEU, K. E., MUSIL, F. J. & WHITNEY, D. R. (1962). *Acta Cryst.* **15**, 1292.
DUMOND, J. W. M. & HOYT, A. (1930). *Phys. Rev.* **36** 1702.
EASTABROOK, J. N. (1952). *Brit. J. Appl. Phys.* **3**, 349.
LIPSON, H. & WILSON, A. J. C. (1941). *J. Sci. Instrum* **18**, 144.
PIKE, E. R. (1957). *J. Sci. Instrum* **34**, 355.
PIKE, E. R. & WILSON, A. J. C. (1959). *Brit. J. Appl. Phys.* **10**, 57.
SCHWARZSCHILD, M. M. (1928). *Phys. Rev.* **32**, 162.
SPENCER, R. C. (1931). *Phys. Rev.* **38**, 622.
STRAUMANIS, M. E. & IEVINS, A. (1940). *The precision determination of lattice constants by the asymmetric method.* Originally published in German by Julius Springer, Berlin, and translated by K. E. Beu as USAEC Report GAT-T-643, April 15, 1959.
STRAUMANIS, M. E. & WENG, C. C. (1955). *Acta Cryst.* **8**, 367.
TAYLOR, A. & SINCLAIR, H. (1945). *Proc. Phys. Soc.* **57**, 126.

Acta Cryst. (1964). **17**, 645

Precise and Accurate Lattice Parameters by Film Powder Methods. IV. Theoretical Calculation of Axial (Vertical) Divergence Profiles, Centroid Shifts, and Variances for Cylindrical Powder Diffraction Cameras

BY J. I. LANGFORD
University College, Cardiff, Wales

E. R. PIKE
Royal Radar Establishment, Malvern, Worcs., England

AND K. E. BEU,
Goodyear Atomic Corporation, Piketon, Ohio, U.S.A.*

(*Received* 11 *June* 1963)

An analytic method, based on an expansion of Eastabrook (1952) to the first power in the deviation from the Bragg angle, is used to derive the axial-divergence line profiles, centroid shifts and variances for cylindrical powder cameras. Numerical values and profiles are given for the modified 5·76 cm Philips camera and input collimator described by Beu, Musil & Scott (1962). The profiles are compared with those obtained by Beu, Landstrom, Whitney & Pike (1964) (preceding paper) who used a graphical method, based on exact equations, for the same calculation.

Excellent agreement is found over all but the extreme ends of the angular range, $\sim 2\theta$ greater than 175° and less than 10°. At these extreme angles the graphical method is expected to give superior results, since the expansions used in the analytical approach become more slowly convergent. It is shown, however, that at the high-angle end the differences are too small to be of practical account, although at low Bragg angles the differences might be measurable.

The displacement of the centroid is found to be $-0{\cdot}025°(2\theta)$ at $10°(2\theta)$ falling to zero at about 130°, and is 0·005° at 170°. The corresponding root-mean-square breadths at these angles are, respectively, $0{\cdot}030°(2\theta)$, a minimum of about 0·002° and 0·006°.

1. Introduction

A short review of previous work on axial-divergence effects has been given by Beu, Landstrom, Whitney & Pike (1964) (preceding paper) with the conclusion that no quantitative methods for the evaluation of these effects in film powder cameras were previously available. This was remedied by a graphical calculation of line profiles based on the exact geometrical relationship between primary and diffracted rays given

* Under Contract AT-(33-2)-1 with the U.S. Atomic Energy Commission.